analytical chemistry

pubs.acs.org/ac Article

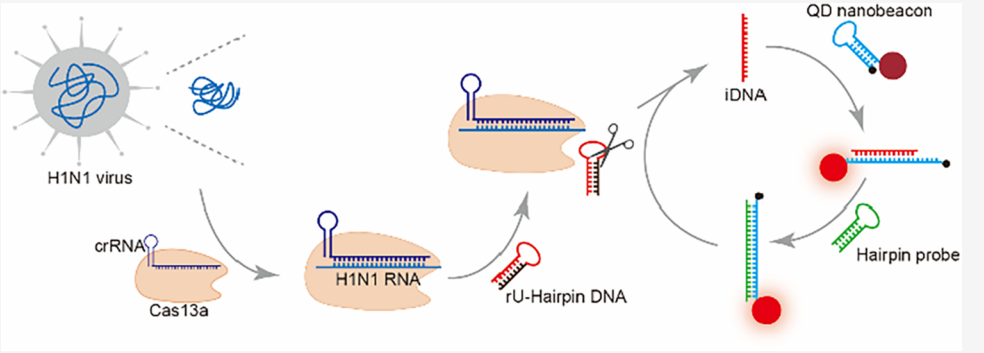
# CRISPR/Cas13a-Driven Catalytic Hairpin Assembly of a Quantum Dot Nanobeacon for Viral RNA Detection

Yeling Yang,[‖] Yucheng Liu,[‖] Hui Xu, Fuxiang Zhou, Xinghu Ji, and Zhike He*

Cite This: https://doi.org/10.1021/acs.analchem.5c08146 Read Online

ACCESS | Metrics & More | Article Recommendations | Supporting Information

Downloaded via SHANGHAI NORMAL UNIV on May 6, 2026 at 13:45:38 (UTC).
See https://pubs.acs.org/sharingguidelines for options on how to legitimately share published articles.




**ABSTRACT:** Influenza A (H1N1), which is a highly contagious respiratory pathogen, poses a serious public health threat. Its effective control necessitates rapid and accurate detection methods. Here, we developed a novel quantum dot (QDs) nanobeacon-based biosensor that synergistically integrates the precise target recognition and trans-cleavage activity of CRISPR/Cas13a with the isothermal, enzyme-free signal amplification power of catalytic hairpin assembly (CHA) for sensitive detection of H1N1 RNA. This system achieves dual signal amplification, enabling detection with a remarkably low limit of detection (LOD) of 95.2 aM within 40 min. Excellent specificity distinguishes H1N1 from other common influenza viruses. Crucially, the programmability of crRNA endows the method with broad versatility. Beyond influenza virus detection, it was successfully applied to SARS-CoV-2 RNA detection, achieving an LOD of 87.0 aM, demonstrating its potential for diverse pathogen diagnostics. These results collectively demonstrate the high performance and adaptability of this diagnostic platform, highlighting its significant promise for future applications in the rapid and sensitive detection of diverse viral pathogens.

## INTRODUCTION

Influenza virus is an enveloped negative-strand RNA virus.[1] Most warm-blooded animals, ranging from wild waterfowl to poultry and humans, can serve as hosts. Infected individuals may present with diverse clinical manifestations from asymptomatic infection or mild conjunctivitis to fulminant pneumonia even the death, demonstrating significant morbidity and mortality rates.[2] Currently, influenza viruses are classified into types A, B, C, and D,[3,4] with influenza A virus (H1N1) being the most severe and lethal subtype. This pathogen has caused transnational transmission events, emerging as a critical global public health concern.[5,6] The gold-standard diagnostic method remains quantitative reverse transcription-polymerase chain reaction (RT-qPCR) using throat/nasal swab samples.[7−10] While RT-qPCR holds high sensitivity and specificity, it necessitates precise thermal cycling instrumentation for repeated processes of denaturation-annealing-amplification to achieve target amplification. Consequently, developing simple, rapid, and ultrasensitive diagnostic approaches for H1N1 RNA detection holds great significance for disease control.

CRISPR (Clustered Regularly Interspaced Short Palindromic Repeats) is an important immune defense system for bacteria and archaea. When crRNA binds to Cas protein forming the CRISPR/Cas complex, it can target and recognize exogenous nucleic acids.[11] The CRISPR/Cas12 and CRISPR/Cas13 systems have been used for nucleic acid detection due to their precise target recognition ability and trans-cleavage properties for nontarget nucleic acids.[12−14] Doudna et al.[15] developed the DETECTR (DNA endonuclease-targeted CRISPR trans reporter) method by integrating recombinase polymerase amplification (RPA) with CRISPR/Cas12a, achieving attomolar (aM) sensitivity. Zhang et al.[16] established the SHERLOCK (Specific High-Sensitivity Enzymatic Reporter UnLOCKing) platform using RPA-CRISPR/Cas13a

Received: December 23, 2025
Revised: April 25, 2026
Accepted: April 28, 2026

ACS Publications © XXXX American Chemical Society

dual signal amplification for Zika and dengue virus detection with 2 aM limit of detection (LOD). These methods typically require previous enzymatic amplification followed by CRISPR/Cas-mediated recognition and trans-cleavage of the amplification product, further realizing the signal enhancement. However, these methods often involve complex primer design, multiple enzymatic components, and dual-modified RNA reporters, thus increasing the operational complexity and cost. CRISPR/Cas13 is a system that targets RNA and has trans-cleavage effect on single stranded RNA. Zhou et al.[17] engineered a colorimetric biosensor by combining CRISPR/Cas13 with hybridization chain reaction (HCR) for H1N1 RNA detection. Activated Cas13a cleaves RAN probes with UUU special sequences to initiate HCR, eliminating the need for dual-modified RNA reporters while enhancing the sensitivity through dual signal amplification. Different from HCR, catalytic hairpin assembly (CHA) as an enzyme-free isothermal amplification technique enables cyclic catalyst regeneration. The initiator strands catalyze hairpin opening, form stable duplex structures with secondary hairpins, and then dissociate to perpetuate the reaction cycle. This simple, efficient methodology has been widely adopted in CRISPR-based molecular diagnostics.[18−20]

Quantum dots (QDs) are semiconductor nanomaterials with broad excitation spectra, narrow emission bands, and high quantum yields.[21] Due to the programmability of DNA, DNA-functionalized QDs are often used in probe construction and show exceptional promise in molecular diagnostics.[22,23] There are many methods to modify DNA on the surface of QDs,[24] such as carbodiimide chemical method by coupling the amino-modified DNA to carboxylated QDs,[25] functionalization of QDs via thiolated DNA based on metal−ligand coordination, and direct synthesis of DNA-QDs with phosphorylated phosphorothioated DNA (ps-po DNA).[26] Notably, DNA-templated direct synthesis of DNA-QDs exhibit superior water solubility, tunable valence states, and high quantum yields, showing obvious advantages in the construction of biosensing probes.

Herein, we developed a rapid, sensitive platform for H1N1 RNA detection by integrating QD nanobeacon probes with CRISPR/Cas13 and CHA. First, we employ a seed-mediated growth approach to construct CdTe/CdS QD-DNA-BHQ2 nanobeacons (QD-NBs) using ps-po DNA-BHQ2. The CdTe/CdS QDs demonstrate an exceptional thermal stability and fluorescence intensity. Then, we design a uridine-modified hairpin DNA (rU-HD) containing three functional domains: (1) an iDNA segment initiating subsequent CHA reactions, (2) the rU motifs susceptible to Cas13a/crRNA complex trans-cleavage, and (3) complementary regions for duplex formation. In the presence of the target, Cas13a/crRNA complexes are activated, then nonspecifically cleaving rU-HD to release iDNA, which further initiates a catalytic cycle to form stable QD-NB/HP duplexes. The stable QD-NB/HP duplexes cause the spatial separation of BHQ2 quenchers from QDs, resulting in the recovery of the fluorescence signal. The system can be used for the detection of H1N1 RNA and H1N1 virus in saliva, which holds great potential for the detection of the H1N1 influenza virus in complex matrices.

## EXPERIMENTAL SECTION

### Reagents and Materials

LbuCas13a protein was purchased from Biolifesci Co., Ltd. (Guangzhou, China). 4SGelred nucleic acid stain (100,00× in water), premixed TBE buffer powder (1×), 2× TBE loading buffer, gel loading buffer (6×), and 40% acrylamide/bis-acrylamide solution (40% Acryl/Bis, 29:1) were purchased from Sangon Biotechnology Co. Ltd. (Wuhan, China). Potassium chloride solution (KCl, RNase-free, 1 M) was obtained from Heowns BioChem Technologies (Tianjin, China). Sodium chloride solution (NaCl, RNase-free, 5 M) and magnesium chloride solution ($MgCl_2$, RNase-free, 1 M) were purchased from Thermo Fisher Scientific (Waltham, MA, USA). Tris-HCl buffers of different pH values (RNase-free, 1 M) were obtained from Yuanye Bio-Technology Co., Ltd. (Shanghai, China). Cadmium chloride ($CdCl_2$·2.5H2O, AR), tellurium powder (Te, 99.999%), and sodium hydroxide (NaOH, AR) were purchased from Sinopharm Chemical Reagent Co., Ltd. (Shanghai, China). Sodium borohydride (NaBH4, 99.99%), N-acetylcysteine (NAC, ≥99%), 3-mercaptopropionic acid (MPA, ≥99%), and tris(2-carboxyethyl) phosphine hydrochloride solution (TCEP, 0.5 M) were obtained from Sigma-Aldrich (St. Louis, MO, USA). All DNA sequences were ordered from Sangon Biotech (Shanghai, China). The substrate molecules for RNA, crRNA, and labeled RNA cleavage sites (UUUUU) were sourced from Takara Biotech. Inc. (Beijing, China). The sequences of the oligonucleotides are listed in Table S1.

### Characterization

All fluorescence signals were measured with an RF-6000 fluorescence spectrophotometer (Shimadzu, Japan). The ultraviolet−visible (UV−vis) absorption spectra of QDs and DNA-QDs were investigated on a UV-2250 spectrophotometer (Shimadzu, Japan). TEM samples were analyzed by using a JEM 2100 plus transmission electron microscope (JEOL, Japan). The crystalline structures of Cd/Te and CdTe/CdS were analyzed by the PANalytical X'pert Pro X-ray diffraction (XRD). The chemical composition of Cd, Te, C, O, S, and P was characterized by X-ray photoelectron spectroscopy (XPS) on a Thermo Scientific Escalab 250Xi X-ray photoelectron spectroscopy.

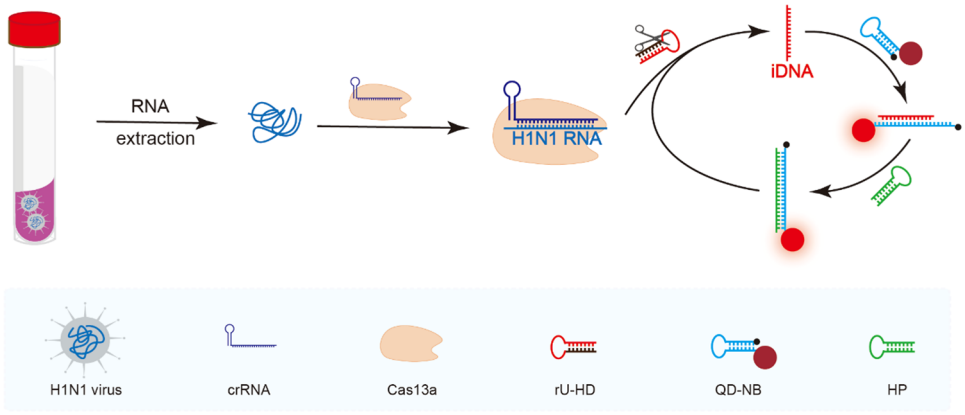
### Synthesis of DNA-Functionalized CdTe/CdS QDs (QD-NB)

The synthesis of CdTe QDs: A freshly prepared NaHTe solution was synthesized by mixing 20 mg Te powder and 11 mg $NaBH_4$ with 1.0 mL deionized water pretreated with $N_2$ bubbling. The mixture was reacted under an ice bath and continuous $N_2$ purging for 4 h, yielding a transparent pale pink solution. For Cd-MPA solution preparation, 0.25 mmol MPA and 0.25 mmol $CdCl_2$ were dissolved in 50 mL of deionized water, and the pH was adjusted to 11.0 using 1 M NaOH. To synthesize CdTe QDs, the Cd-MPA solution was subjected to continuous $N_2$ bubbling for 30 min, followed by rapid injection of 50 μL freshly prepared NaHTe solution. The Cd−Te-MPA mixture was incubated at 4 °C in darkness to facilitate CdTe QD formation. Purification involved adding three volumes of anhydrous ethanol to the QD solution, followed by centrifugation at 10,000 rcf (relative centrifugal force) for 10 min. The resulting precipitate was washed three times with a 1:3 (v/v) ethanol/water solution and finally resuspended in nuclease-free water.

The synthesis of QD-NB: The Cd-NAC solution was prepared by adding 171 mg of $CdCl_2$ and 258 mg of NAC to 40 mL of deionized water, followed by pH adjustment to 9.0. A mixture containing 15 μL of 120 μM CdTe QDs solution, 200 μL of Cd-NAC solution, and 18 nmol of phosphorothioate- and BHQ2-modified DNA (ps-po DNA) was prepared in a total volume of 2 mL. The mixture was transferred to a hydrothermal reactor and heated at 155 °C for 28 min to synthesize DNA-functionalized CdTe/CdS QDs (QD-NB). Purification was performed using the Amicon Ultra-4 centrifugal filter device. The initially purified solution was combined with 450 μL nuclease-free water and centrifuged at 8000*g* for 10 min, with this washing procedure repeated three times. The purified QD-NB was stored at 4 °C in the dark.


https://doi.org/10.1021/acs.analchem.5c08146
Anal. Chem. XXXX, XXX, XXX−XXX

**Scheme 1. Schematic Diagram of the CRISPR/Cas-CHA System for the Detection of H1N1 RNA**



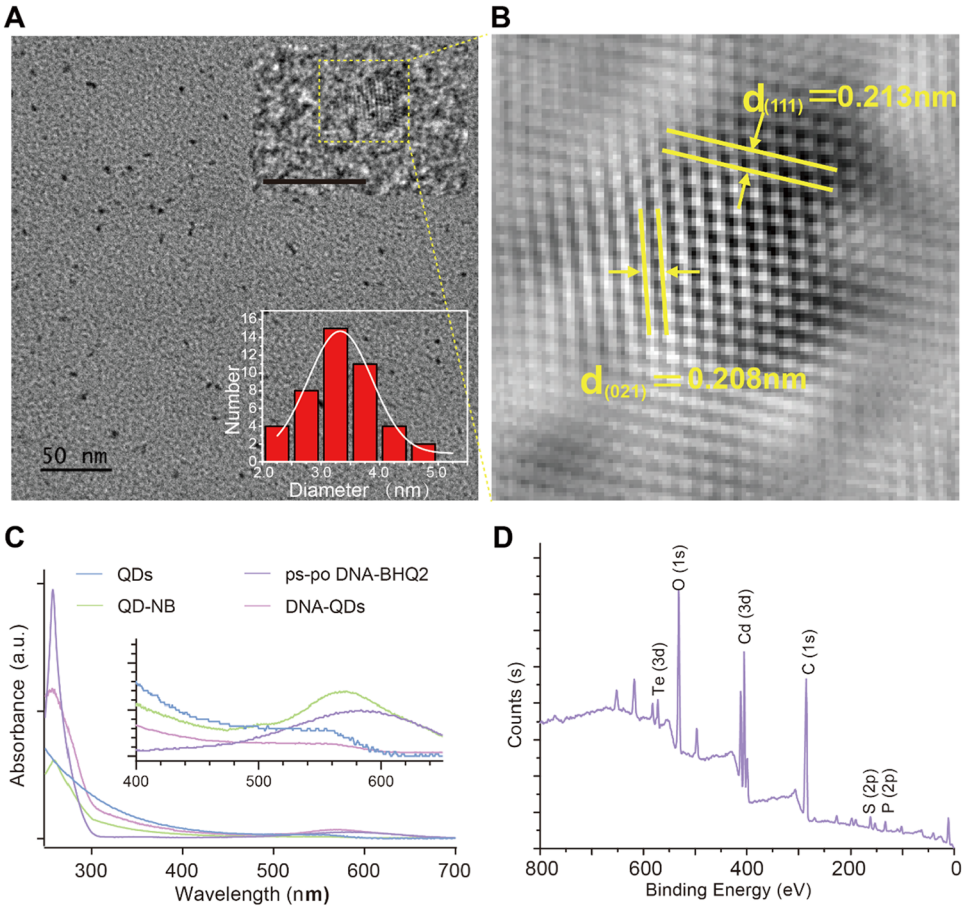




**Figure 1.** (A) TEM imaging of CdTe/CdS QDs; scale bar: 50 nm (inset: HRTEM image of CdTe/CdS QDs (up), scale bar: 5 nm, size distribution of CdTe/CdS QDs (down)). (B) Crystallographic analysis of CdTe/CdS QDs. Two distinct lattice fringes are resolved: a *d*-spacing of 0.213 nm assigned to the (111) plane of CdS and a *d*-spacing of 0.208 nm assigned to the (021) plane of CdS. (C) UV visible absorption spectra of QDs, ps-po DNA-BHQ2, DNA-QDs and QD-NB, respectively. (D) XPS spectra of DNA-CdTe/CdS QDs.

## Detection of H1N1 RNA in Standard Solutions

To facilitate hairpin formation through annealing, rU-HD was denatured at 75 °C for 2 min and gradually cooled to room temperature. QD-NB and HP were denatured at 90 °C for 10 min,[27,28] followed by cooling at room temperature for 30 min to ensure stable hairpin structure formation. A 20 μL Cas13a cleavage reaction system containing H1N1 RNA, 50 nM LbuCas13a, 25 nM crRNA, and 100 nM rU-HD in Cas13 buffer was incubated at 37 °C for 15 min. Subsequently, 1 μM HP and 0.4 μM QD-NB were added to the reaction solution, followed by incubation at room temperature for 25 min.

## Gel Electrophoresis Analysis

A 15% urea-denaturing polyacrylamide gel electrophoresis (PAGE) system was prepared to characterize Cas13a cleavage products. The polymerized gel was preelectrophoresed at a constant voltage of 50 V for 30 min. Subsequently, 5 μL of samples were mixed with 5 μL of 2× TBE loading buffer and loaded into gel wells. Electrophoresis proceeded at 80 V for 100 min. After electrophoresis, the gel was immersed in 1× 4SGelRed staining solution for 5 min and imaged using a ChemiDoc XRS system.

Feasibility of the CRISPR/Cas13a-coupled CHA assay for H1N1 RNA detection was validated by 15% nondenatured polyacrylamide


https://doi.org/10.1021/acs.analchem.5c08146
Anal. Chem. XXXX, XXX, XXX−XXX

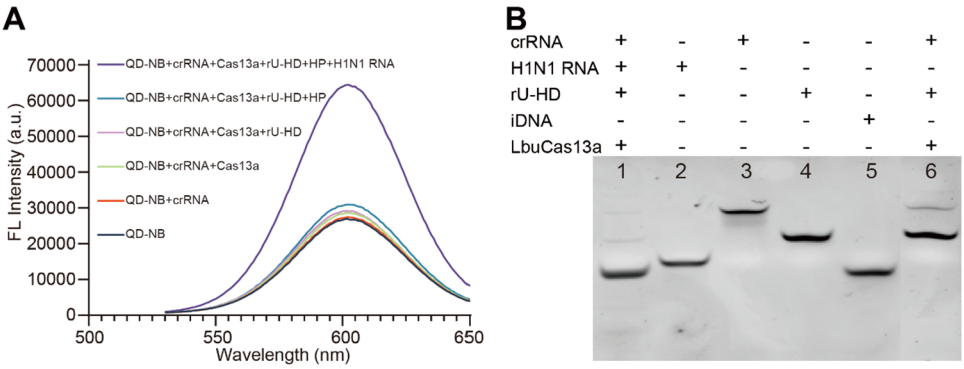



**Figure 2.** (A) Feasibility analysis of the CRISPR/Cas-CHA method (a. QD-NB; b. QD-NB + crRNA; c. QD-NB + crRNA + Cas13a; d. QD-NB + crRNA + Cas13a + rU-HD; e. QD-NB + crRNA + Cas13a + rU-HD + HP; f. QD-NB + crRNA + Cas13a + rU-HD + HP + H1N1 RNA). (B) Analysis of Cas13a/crRNA activity in the presence of target RNA (1. Cas13a + crRNA + H1N1 RNA + rU-HD; 2. H1N1 RNA; 3. crRNA; 4. rU-HD; 5. iDNA; 6. Cas13a + crRNA + rU-HD).

gel electrophoresis. The electrophoresis buffer was prepared by using commercially available premixed TBE buffer powder. Samples (5 $\mu$L) were combined with 2 $\mu$L of 6× loading buffer, and 5 $\mu$L of the mixture was loaded per well. Electrophoresis was performed at 110 V for 90 min, followed by gel processing, as described above.

### Analysis of H1N1 RNA in Saliva Samples

Saliva specimens were collected from healthy volunteers. Samples were initially treated with Tris and TCEP, followed by a two-step ribonuclease inactivation procedure: incubation in a 50 °C water bath for 5 min and then transfer to a 95 °C water bath for 5 min. After inactivation, the mixture was centrifuged at 12,000 rpm for 5 min, and the supernatant was then collected for downstream reactions. The supernatant was diluted 100-fold with nuclease-free water and spiked with H1N1 RNA at varying concentrations. Detection of H1N1 RNA in saliva followed the same protocol described in Detection of H1N1 RNA in Standard Solutions.

Virus RNA was extracted from H1N1-infected MDCK cells using the Hipure Virus DNA/RNA kit (R4173-03, Magen Biotech Co., Ltd., Guangzhou, China). Extraction of influenza A (H1N1) virus RNA was performed at the Wuhan Institute of Virology, Hubei, China. Virus RNA detection procedures followed the same protocol described in Synthesis of DNA-Functionalized CdTe/CdS QDs (QD-NB).

## RESULTS AND DISCUSSION

### Principle of the CRISPR/Cas-CHA System for Virus RNA Assay

The hemagglutinin gene fragment of influenza virus H1N1 was selected as the target RNA. The designed crRNA comprises two functional domains: one for H1N1 RNA recognition and another for LbuCas13a binding to form the Cas13a/crRNA complex. The system operates through two sequential mechanisms: (1) CRISPR/Cas-mediated target-activated trans-cleavage and (2) CHA driven by initiator DNA (iDNA) to modulate quantum dot beacons. As illustrated in Scheme 1, upon H1N1 RNA recognition, the Cas13a/crRNA complex executes cis-cleavage of the target RNA, subsequently initiating trans-cleavage activity at the UUUUU loop region of the engineered rU-HD hairpin. This releases iDNA, which hybridizes with QD-NB to form iDNA/QD-NB hybrids. The exposed sticky ends of these hybrids open hairpins, generating QD-NB/HP duplexes while regenerating free iDNA. The liberated iDNA perpetuates the CHA cycle, enabling exponential amplification that restores QD fluorescence.

### Characterization of DNA-Functionalized CdTe/CdS QD-NB

The morphologies of CdTe QDs and CdTe/CdS QDs were characterized using transmission electron microscopy (TEM) (Figures 1A,B and S1). Both CdTe/CdS QDs and CdTe QDs are uniformly dispersed and exhibit spherical morphologies. As determined by particle size analysis, CdTe/CdS QD exhibits an average diameter of 3.28 ± 0.03 nm, which is larger than that of CdTe QDs (1.26 ± 0.34 nm) (Figure S1B). The inserted HRTEM image distinctly displays lattice fringes of the QD-NB. The HRTEM image of CdTe/CdS QDs (Figure 1B) shows two distinct lattice fringes: a *d*-spacing of 0.213 nm assigned to the (111) plane of CdS, and a *d*-spacing of 0.208 nm assigned to the (021) plane of CdS. The HRTEM image of CdTe QDs (Figure S1) shows a distinct lattice fringe with a *d*-spacing of 0.215 nm, assigned to the (200) plane of CdTe. As shown in Figure S2, the diffraction pattern of CdTe QDs matches well with the simulated pattern derived from the standard card data of CdTe. In addition, the diffraction pattern of CdTe/CdS QDs is also presented, where the diffraction angles align with the characteristic peaks from the CdTe/CdS XRD standard card, confirming the successful growth of the CdS shell.

To verify that DNA was successfully conjugated onto the surface of the quantum dots, we characterized the DNA-functionalized QDs using UV−vis absorption spectroscopy, X-ray photoelectron spectroscopy (XPS), and TEM. As shown in Figure 1C, absorption peaks at approximately 260 nm were observed for ps-po DNA-BHQ2 (containing phosphorothioate and BHQ2 modifications), DNA-QDs, and QD-NB. Both DNA-QDs and QDs exhibited an absorption peak at approximately 560 nm, whereas the absorption peak of QD-NB was red-shifted to approximately 580 nm, which may be attributed to the overlap and shielding effect of the absorption peak of BHQ2. As shown in Figure 1D, distinct Te (3d), O (1s), Cd (3d), C (1s), S (2p), and P (2p) peaks are observed. The presence of the P (2p) peak confirms the successful DNA modification of QDs. The UV−vis absorption spectroscopy and XPS confirmed the successful modification of DNA. Futhermore, DNA-QD1 and DNA-QD2 were synthesized using complementary ps-po DNA1 and ps-po DNA2, respectively. Upon mixing DNA-QD1 and DNA-QD2 at a 1:1 ratio to facilitate quantum dot assembly, TEM characterization of the assembled structure (Figure S3) demonstrates dumbbell-shaped architectures, indicating the successful preparation of single DNA-modified QDs.


https://doi.org/10.1021/acs.analchem.5c08146
Anal. Chem. XXXX, XXX, XXX−XXX

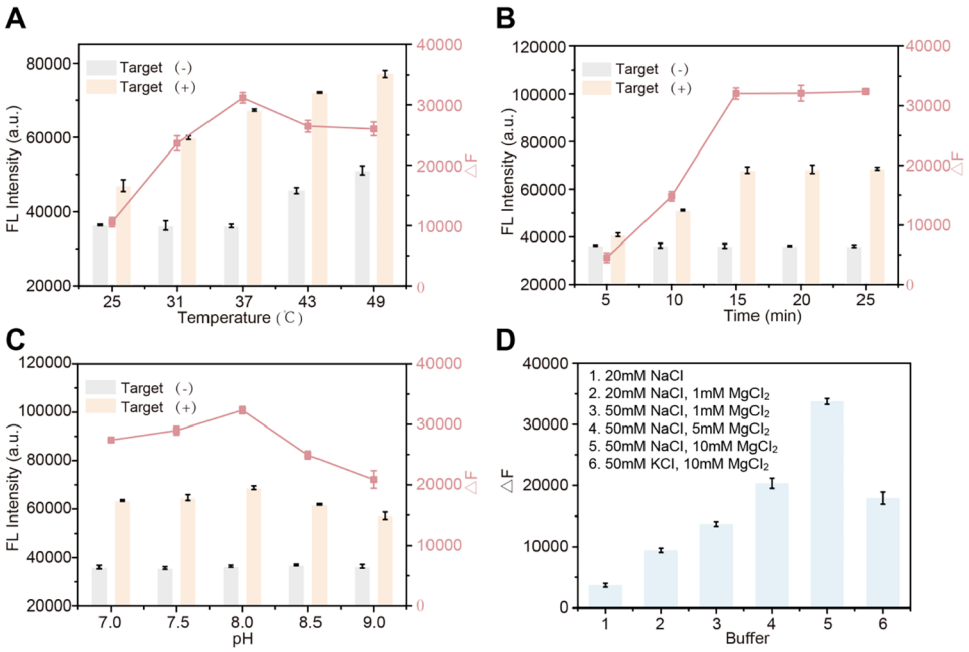



**Figure 3.** Optimization of incubation temperature (A), incubation time (B), pH (C), and composition of the Cas13a/crRNA complex trans lysis buffer (D).

## Feasibility of the CRISPR/Cas-CHA System for H1N1 RNA Detection

To validate the feasibility of the CRISPR/Cas-CHA system for H1N1 RNA detection, fluorescence emission spectra of the solutions under varying conditions were investigated. Compared to control groups lacking H1N1 RNA, rU-HD, or HP2, only the complete system containing the Cas13a/crRNA complex, H1N1 RNA, rU-HD, HP2, and QD-NB exhibited significant signal recovery (Figure 2A). As shown in Figure 2B, the emerged band in Lane 1 demonstrates migration velocity identical to that of the iDNA band in Lane 5, confirming that the Cas13a/crRNA complex mediates trans-cleavage of rU-HD and releases iDNA in the presence of H1N1 RNA.

Since gel electrophoresis cannot distinguish between quantum dot beacon-HP2 hybridization products and the quantum dot beacon itself, HP1 with identical sequences was substituted for the quantum dot beacon to validate the feasibility of Cas13a/crRNA trans-cleavage products triggering the CHA reaction. As illustrated in Figure S4, three distinct bands corresponding to HP1-HP2, iDNA, and ssDNA are observed in Lane 1 compared to those in Lane 2. Theoretically, iDNA exhibits faster migration than ssDNA but slower than HP1-HP2, while the ssDNA band displays lower intensity relative to HP1-HP2 and iDNA bands. These observations align with our PAGE experimental results, demonstrating that substrate rU-HD cleavage and subsequent iDNA release—prerequisites for initiating the CHA reaction to form HP1-HP2—occur exclusively in the presence of target RNA.

## Construction and Optimization of the CRISPR/Cas-CHA System

The CRISPR/Cas-CHA system comprises two key components: (1) enzymatic cleavage of virus RNA and substrate rU-HD by CRISPR/Cas13a and (2) CHA triggered by iDNA (released via Cas13a trans-cleavage) between the quantum dot beacon and HP2. The first step relies on the specific recognition of virus RNA by the Cas13a/crRNA complex. Upon target binding and cleavage, activated Cas13a which exhibits ribonuclease activity cleaves the uracil-ribonucleotide-modified substrate hairpin (rU-HD, where UUUUU is positioned in the loop region). Cleavage of rU-HD destabilizes its duplex structure under experimental conditions, thereby releasing the initiator strand iDNA. The second step involves iDNA-triggered CHA, wherein the quantum dot beacon unfolds and hybridizes with HP2 to form a more stable duplex, resulting in a fluorescence signal recovery. Consequently, the reaction conditions for both steps were optimized separately.

First, the concentrations of Cas13a and crRNA in the cleavage reaction were optimized. As shown in Figure S5A, background signals remained stable with the increasing Cas13a concentration, while quantum dot fluorescence recovery intensified significantly. The fluorescence intensity variation ($\Delta F$) of the CRISPR/Cas-CHA system plateaued at 50 nM Cas13a. Figure S5B demonstrates that $\Delta F$ initially increased and then slightly decreased with the rising crRNA concentration. At 25 and 30 nM crRNA, $\Delta F$ values were comparable and maximized under optimized conditions. Thus, subsequent experiments employed 50 nM Cas13a and 25 nM crRNA.

We further optimized the structure of substrate rU-HD (Figure S5C). Experiments using rU-HD with varying stem lengths revealed significantly higher background signals for substrates with an 8-bp stem compared to those with 10, 12, or 14 bp stems. This suggests instability in the duplex structure or unintended mutual activation between rU-HD (8-bp stem) and QD-NB, elevating background noise. The most pronounced quantum dot signal recovery occurred with a 12 bp rU-HD stem, indicating optimal performance for rU-HD12 as a substrate. A marked decrease in $\Delta F$ was observed for the 14-bp rU-HD stem, likely due to its stable postcleavage duplex structure hindering QD-NB activation and subsequent CHA initiation.

Subsequently, we optimized the temperature, duration, pH, and reaction buffer for the enzymatic cleavage step. The impact of five temperatures (25, 31, 37, 43, and 49 °C) on CRISPR/


https://doi.org/10.1021/acs.analchem.5c08146
Anal. Chem. XXXX, XXX, XXX−XXX

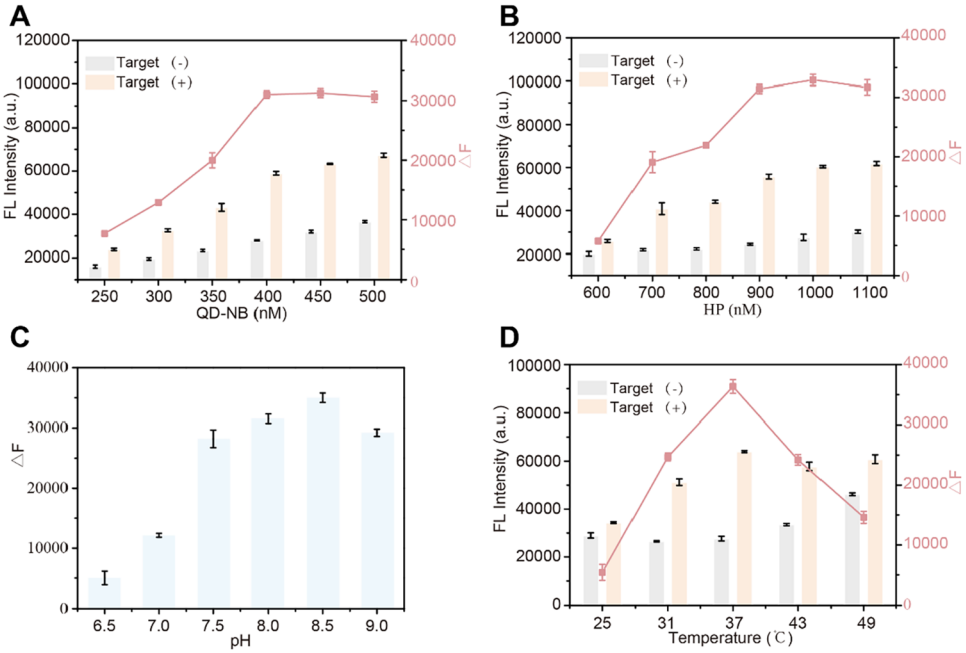



**Figure 4.** Optimization of QD-NB concentration (A), HP concentration (B), CHA reaction pH (C), and CHA reaction temperature (D).

Cas13a trans-cleavage was evaluated. As shown in Figure 3A, $\Delta F$ of the CRISPR/Cas-CHA system initially increased and then decreased with rising temperature, peaking at 37 °C (optimal temperature). Elevated background signals at 43 and 49 °C may stem from reduced substrate stability under higher temperatures. Figure 3B demonstrates that fluorescence intensity increased and plateaued with reaction time (5−25 min) in the presence of H1N1 RNA, while the background remained constant. Maximum $\Delta F$ was achieved after 15 min of Cas13a incubation, establishing 15 min as the optimal duration. Optimization of the cleavage reaction buffer (10×) is detailed in Figure 3C. The most significant fluorescence recovery occurred at pH 8.0. Neutral (pH 7.0) and mildly alkaline (pH 7.5) conditions slightly reduced $\Delta F$, while pH > 8.5 substantially decreased $\Delta F$, indicating diminished enzymatic activity under alkaline conditions. As shown in Figure 3D, a negligible $\Delta F$ in the absence of $Mg^{2+}$ (despite virus RNA presence) indicates the critical role of $Mg^{2+}$ in Cas13a cleavage activity. Maximum $\Delta F$ was attained with a buffer containing 50 mM NaCl and 10 mM $MgCl_2$. Substituting KCl for NaCl significantly reduced the $\Delta F$. Thus, the optimal cleavage buffer composition is Tris-HCl (pH 8.0) with 50 mM NaCl and 10 mM $MgCl_2$.

To further optimize the detection performance of the CRISPR/Cas-CHA system, we investigated the concentrations of the QD-NB and hairpin probe (HP), as well as the pH, temperature, and reaction time of the CHA solution. As shown in Figure 4A, with increasing concentrations of QD-NB, both the background and signal of the CRISPR/Cas-CHA system increased, while the $\Delta F$ value initially rose and then plateaued. The optimal QD-NB concentration was determined to be 400 nM. Figure 4B illustrates the effect of the HP concentration on the assay. When the HP concentration exceeded 900 nM, the $\Delta F$ value of the CRISPR/Cas-CHA system significantly increased, reaching its maximum at 1000 nM. Therefore, the optimal reaction concentrations for QD-NB and HP were determined to be 400 and 1000 nM, respectively. Figure 4C presents the detection of H1N1 RNA by the CRISPR/Cas-CHA system under six different pH conditions (6.5, 7.0, 7.5, 8.0, 8.5, and 9.0). The results indicated that under acidic (pH 6.5) and neutral (pH 7.0) conditions, the $\Delta F$ value was minimal, likely due to the instability of the QDs and compromised fluorescence intensity under these conditions. In contrast, under alkaline conditions (pH 7.5, 8.0, 8.5, and 9.0), the fluorescence of the QDs recovered significantly, with the optimal pH being 8.5, where the $\Delta F$ value peaked. Additionally, the influence of five different temperatures (25, 31, 37, 43, and 49 °C) on the CHA reaction of the CRISPR/Cas-CHA system was examined. As depicted in Figure 4D, the background signal at 43 and 49 °C was notably higher than that at 25, 31, and 37 °C, suggesting that the hairpin structures in the solution could not maintain stable stem-loop conformations at elevated temperatures, leading to increased background. At 25 °C, the $\Delta F$ value was low, indicating that low temperatures inhibited the CHA reaction. The maximum $\Delta F$ value was observed at 37 °C, establishing this as the optimal reaction temperature. At 43 and 49 °C, the $\Delta F$ value exhibited a declining trend, attributable to both the elevated background and the adverse effects of high temperatures on quantum dot fluorescence. Lastly, we determined the optimal reaction time for the CHA process. As shown in Figure S5D, the $\Delta F$ value initially increased and then decreased, with the peak response occurring at 25 min. In addition, as shown in Figure S6, we examined the time-dependent fluorescence intensities of the system at different concentrations (1 pM, 1 nM, and 100 nM). After the addition of CHA primers and QD-NB probes, the signal increased over time and reached saturation within 25 min, and the reaction rate increased with the higher target concentrations. Since the CRISPR reaction required 15 min, the total assay time was 40 min, demonstrating that detection of influenza virus H1N1 RNA could be achieved within 40 min.


https://doi.org/10.1021/acs.analchem.5c08146
Anal. Chem. XXXX, XXX, XXX−XXX

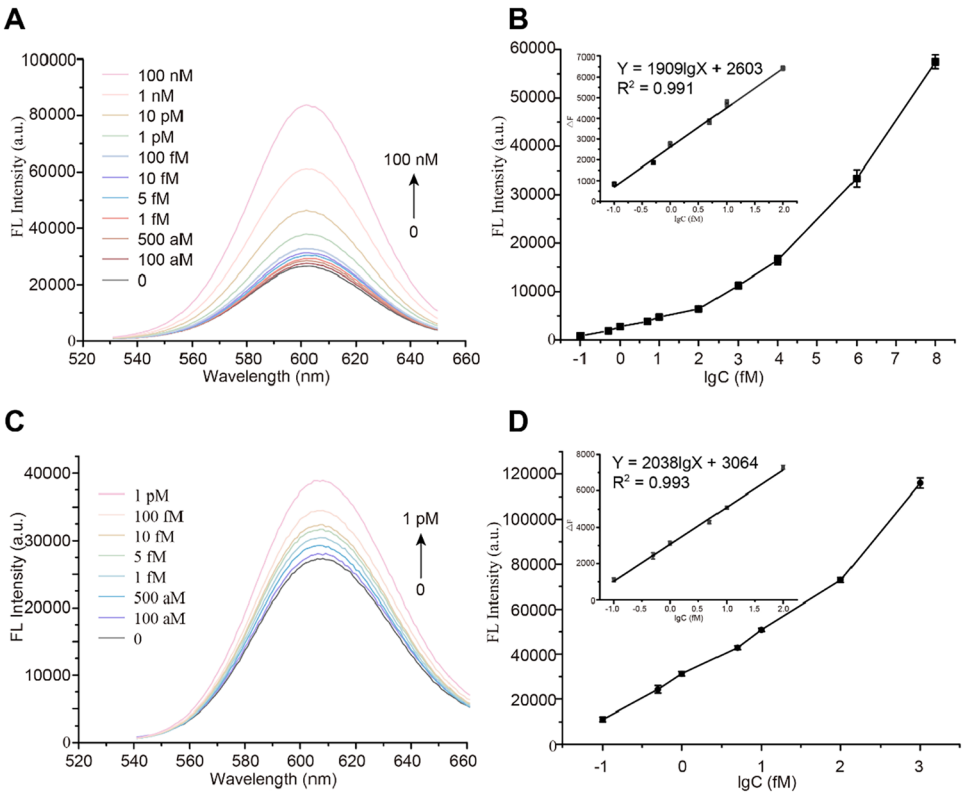



**Figure 5.** (A) Fluorescence spectra of H1N1 RNA at different concentrations. (B) Curve relationship between $\Delta F$ and the logarithm of H1N1 RNA concentration (Inset: linear relationship between $\Delta F$ and the logarithm of H1N1 RNA concentration). (C) Fluorescence spectra of SARS-CoV-2 RNA at different concentrations. (D) Curve relationship between $\Delta F$ and the logarithm of SARS-CoV-2 RNA concentration (Inset: linear relationship between $\Delta F$ and the logarithm of SARS-CoV-2 RNA concentration).

## QD-NB-Based CRISPR/Cas-CHA System for Virus RNA Detection

Under the optimized experimental conditions, we evaluated the detection performance of the CRISPR/Cas-CHA system for H1N1 RNA detection. As the concentration of H1N1 RNA increased, more Cas13a/crRNA complexes were activated, leading to a sharp rise in the concentration of trans-cleaved iDNA, which subsequently triggered additional CHA reactions between QD-NB and HP2. As shown in Figure 5A, with an increasing target concentration, more beacons were opened, resulting in a stronger recovery of the fluorescence signal. Figure 5B demonstrates that within the range of 1 pM to 100 nM H1N1 RNA, the increase in $\Delta F$ became significantly more obvious. Notably, in the range of 100 aM to 100 fM, $\Delta F$ exhibited an excellent linear relationship with the logarithm of the H1N1 RNA concentration, following the regression equation: $Y = 1909 \lg X + 2603$ ($R^2 = 0.991$). The limit of detection (LOD) was determined to be 95.2 aM.

To validate the versatility of this method, we applied it to the detection of SARS-CoV-2 RNA. We examined the changes in fluorescence intensity at target concentrations of 0, 100 aM, 500 aM, 1 fM, 5 fM, 10 fM, 100 fM, and 1 pM. As illustrated in Figure 5C, the fluorescence signal recovered progressively with increasing target concentration. Figure 5D reveals that within the range of 100 aM to 100 fM, $\Delta F$ maintained a strong linear correlation with the logarithm of the target RNA concentration, described by the regression equation $Y = 2038 \lg X + 3064$ ($R^2 = 0.993$). The LOD for SARS-CoV-2 RNA was calculated to be 87.0 aM. Furthermore, when compared with other methods (Table S2), our approach demonstrated a significantly lower detection limit, highlighting its superior sensitivity.

## Specificity of CRISPR/Cas13a for H1N1 RNA Detection

Owing to the programmability of crRNA and the high cleavage activity of Cas13a, recent studies on the CRISPR/Cas13a system have primarily focused on combining it with enzyme-assisted nucleic acid amplification techniques. These approaches typically involve preamplification of target nucleic acids before introducing the CRISPR/Cas13a system to improve the sensitivity through its activated nuclease activity toward amplification products. However, these methods have overlooked another significant advantage of the CRISPR/Cas13a system, its exceptional specificity in target nucleic acid recognition. In this study, we fully leveraged this inherent advantage of the CRISPR/Cas13a system for H1N1 RNA detection. The crRNA, designed based on the H1N1 RNA sequence, specifically targets and binds to the complementary RNA in solution, thereby activating Cas13a upon target cleavage. In contrast, nontarget nucleic acids cannot form complementary base pairing with the spacer region of crRNA, remaining unrecognized and failing to activate Cas13a. Consequently, the rU-HD in solution remains uncut, maintaining its stable stem-loop structure, and no CHA reaction occurs.

We first evaluated the ability of the CRISPR/Cas-CHA system to discriminate single-base mismatches (Figure 6A,B). As shown in Figure 6B, single-nucleotide mismatches did not cause significant changes in the fluorescence signal, indicating that this method cannot distinguish single-base differences but holds promise for application in broad-spectrum viral screen-


https://doi.org/10.1021/acs.analchem.5c08146
Anal. Chem. XXXX, XXX, XXX−XXX

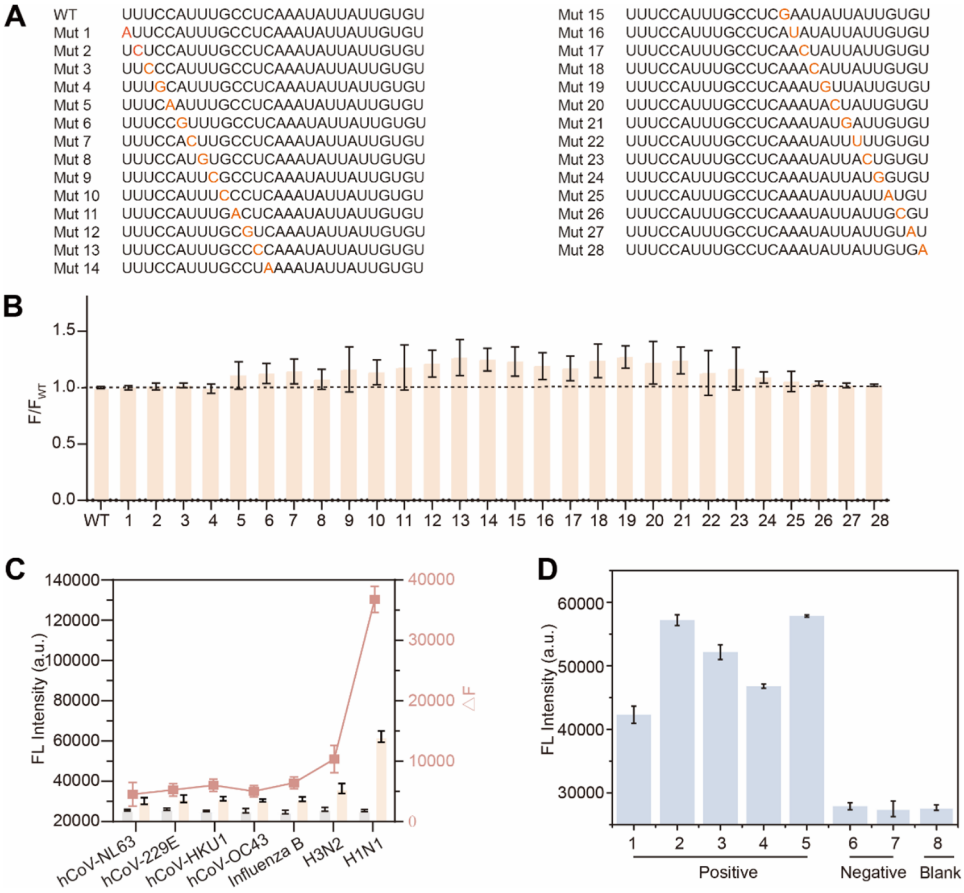



**Figure 6.** (A) Wild-type (WT) H1N1 RNA sequence and its single-base mutant RNA sequence. (B) Fluorescence intensity ratio analysis of a mismatched target to H1N1 RNA. (C) Specificity of the CRISPR/Cas-CHA system for detecting H1N1 virus. (D) Comparative fluorescence intensity of H1N1 virus positive and negative samples.

ing. Furthermore, we evaluate the specificity of the CRISPR/Cas-CHA system for H1N1 virus detection, we selected six RNA viruses which are known to infect humans and can cause common cold symptoms: human coronavirus 229E (hCoV-229E), human coronavirus HKU1 (hCoV-HKU1), human coronavirus NL63 (hCoV-NL63), human coronavirus OC43 (hCoV-OC43), influenza B and influenza A subtype H3N2. As shown in Figure 6C, when detecting the H1N1 virus, the CRISPR/Cas-CHA system exhibited significant signal recovery. In contrast, the $\Delta F$ values remained minimal when detecting hCoV-HKU1, hCoV-229E, hCoV-NL63, hCoV-OC43, influenza B and influenza A subtype H3N2, respectively, demonstrating the excellent specificity of this method.

## Real Sample Analysis

To validate the feasibility of the CRISPR/Cas-CHA system for RNA detection in real samples, a spike-in recovery experiment was conducted in the saliva samples obtained from healthy donors in our laboratory. First, the pretreatment of samples was to eliminate the influence of ribonucleases. Subsequently, varying concentrations of H1N1 RNA were added to the pretreated saliva samples, and the established method was employed for detection. The results are presented in Table 1. The spike-in recovery rates ranged from 84.0 to 117.4%, with relative standard deviation (RSD) values below 10.2%.

To further verify the effectiveness of the proposed CRISPR/Cas-CHA system for practical sample detection, it was utilized to detect the H1N1 influenza virus. Samples 1−5 were extracted positive samples containing H1N1 virus, samples 6 and 7 were negative samples, and sample 8 served as the control group. As shown in Figure 6D, a significant difference was observed between the detection results of the positive and negative samples. These results demonstrate that the experimental method can accurately detect the target RNA within complex RNA samples. Consequently, the method proposed in this work exhibits potential applicability for the detection of the H1N1 influenza virus in complex biological matrices.

**Table 1. Detection of Saliva Samples by the CRISPR/Cas-CHA System**

| target | sample | added (fM) | found (fM) | recovery (%) | RSD (%) ($n$ = 3) |
|---|---|---|---|---|---|
| H1N1 RNA | 1# | 1.00 | 1.12 | 112.3 | 6.3 |
| | | 5.00 | 4.88 | 97.6 | 5.2 |
| | | 10.0 | 9.79 | 97.9 | 7.3 |
| | | 50.0 | 50.8 | 101.6 | 4.4 |
| | 2# | 1.00 | 0.870 | 87.0 | 10.2 |
| | | 5.00 | 5.20 | 104.1 | 6.9 |
| | | 10.0 | 11.5 | 115.3 | 4.7 |
| | | 50.0 | 55.0 | 110.1 | 7.8 |
| | 3# | 1.00 | 1.17 | 117.4 | 9.6 |
| | | 5.00 | 4.20 | 84.0 | 5.1 |
| | | 10.0 | 10.5 | 105.1 | 6.7 |
| | | 50.0 | 48.0 | 96.0 | 7.9 |


https://doi.org/10.1021/acs.analchem.5c08146
Anal. Chem. XXXX, XXX, XXX−XXX

## CONCLUSIONS

In this work, we developed a quantum dot beacon probe integrated with the CRISPR/Cas system and CHA reaction for sensitive detection of virus RNA. Leveraging the high-specificity sequence recognition capability and trans-cleavage activity of CRISPR/Cas13a, the Cas13a/crRNA complex efficiently cleaves the hairpin probe rU-HD upon target recognition, thereby releasing primer strands to initiate the CHA reaction. The work employs a turn-on fluorescence signal mode, effectively avoiding false-positive results during analytical detection. By synergistically utilizing Cas13a protein and CHA amplification, this system achieves dual signal amplification, significantly enhancing detection sensitivity with a limit of detection as low as 95.2 aM. The entire reaction can be completed within 40 min. Furthermore, the method demonstrates excellent specificity, effectively distinguishing between the H1N1 virus and common influenza virus. More importantly, owing to the programmability of crRNA, this method exhibits remarkable versatility. In addition to the detection of influenza virus RNA, it has been successfully applied to detect COVID-19 SARS-CoV-2 RNA, achieving an LOD of 87.0 aM.

While this method allows for the rapid, sensitive, and specific detection of H1N1 RNA, its potential for multiplexed detection has yet to be fully realized. Leveraging the unique single-excitation, multiple-emission characteristics of quantum dots, which provide an ideal foundation for multiplexed assays, future work could focus on engineering multicolor quantum dot probes for the parallel detection of various viral nucleic acids, thus augmenting the practical applicability and versatility of the platform.

## ASSOCIATED CONTENT

### Supporting Information

The Supporting Information is available free of charge at https://pubs.acs.org/doi/10.1021/acs.analchem.5c08146.

TEM characterization of CdTe QDs (Figure S1); XRD spectra of CdTe QDs and CdTe/CdS QDs (Figure S2); TEM images of DNA-QD1 and DNA-QD2 assemblies (Figure S3); gel electrophoresis analysis of the CRISPR/Cas-CHA system for H1N1 RNA detection (Figure S4); optimization of Cas13a concentration, crRNA concentration, the number of bases in the rU-HD reporter probe, and CHA reaction time (Figure S5); fluorescence kinetic curves of the CRISPR/Cas-CHA system (Figure S6); oligonucleotide sequences used in this study (Table S1); comparison of the analytical performance of the proposed method with other reported methods (Table S2) (PDF)

## AUTHOR INFORMATION


### Corresponding Author

**Zhike He** − *Department of Radiation and Medical Oncology, Hubei Key Laboratory of Tumor Biological Behaviors, and Hubei Cancer Clinical Study Center, Zhongnan Hospital of Wuhan University, Wuhan 430072, China; College of Chemistry and Molecular Sciences, Wuhan University, Wuhan 430072, China;* orcid.org/0000-0002-0082-4056; Phone: +86027-68756557; Email: zhkhe@whu.edu.cn; Fax: +86027-68754067

### Authors

**Yeling Yang** − *College of Chemistry and Molecular Sciences, Wuhan University, Wuhan 430072, China*

**Yucheng Liu** − *Core Facility of Wuhan University, Wuhan University, Wuhan 430072, China*

**Hui Xu** − *Department of Radiation and Medical Oncology, Hubei Key Laboratory of Tumor Biological Behaviors, and Hubei Cancer Clinical Study Center, Zhongnan Hospital of Wuhan University, Wuhan 430072, China*

**Fuxiang Zhou** − *Department of Radiation and Medical Oncology, Hubei Key Laboratory of Tumor Biological Behaviors, and Hubei Cancer Clinical Study Center, Zhongnan Hospital of Wuhan University, Wuhan 430072, China*

**Xinghu Ji** − *College of Chemistry and Molecular Sciences, Wuhan University, Wuhan 430072, China*

Complete contact information is available at: https://pubs.acs.org/10.1021/acs.analchem.5c08146

### Author Contributions

‖Y.Y. and Y.L. contributed equally to this work.


### Notes

The authors declare no competing financial interest.

## ACKNOWLEDGMENTS

This work was supported by the National Natural Science Foundation of China (22174101, 22174102). We thank the Core Facility of Wuhan University for the supporting in Characterization. This project was supported by the General Program of the Natural Science Foundation of Hubei Province (2026AFB611).

## REFERENCES


(1) Sandrock, C.; Kelly, T. Clinical review: update of avian influenza A infections in humans. *Crit. Care* **2007**, *11* (2), No. 209.

(2) Taubenberger, J. K.; Morens, D. 1918 Influenza: the mother of all pandemics. *Emerging Infect. Dis.* **2006**, *12* (1), 15.

(3) Hay, A. J.; Gregory, V.; Douglas, A. R.; Lin, Y. P. The evolution of human influenza viruses. *Philos. Trans. R. Soc., B* **2001**, *356* (1416), 1861−1870.

(4) Molini, U.; Curini, V.; Jacobs, E.; Tongo, E.; Berjaoui, S.; Hemberger, M. Y.; Puglia, I.; Jago, M.; Khaiseb, S.; Cattoli, G.; Dundon, W. G.; Lorusso, A.; Di Giallonardo, F. First influenza D virus full-genome sequence retrieved from livestock in Namibia, Africa. *Acta Trop.* **2022**, *232*, No. 106482.

(5) Cheng, V. C. C.; Kelvin, K. W.; Herman, T.; Ivan, F. N.; Yuen, K. Y. Two years after pandemic influenza A/2009/H1N1: what have we learned? *Clin. Microbiol. Rev.* **2012**, *25* (2), 223−263.

(6) Medina, R. A.; García-Sastre, A. Influenza A viruses: new research developments. *Nat. Rev. Microbiol.* **2011**, *9* (8), 590−603.

(7) Merckx, J.; Wali, R.; Schiller, I.; Caya, C.; Gore, G. C.; Chartrand, C.; Dendukuri, N.; Papenburg, J. Diagnostic accuracy of novel and traditional rapid tests for influenza infection compared with reverse transcriptase polymerase chain reaction. *Ann. Intern. Med.* **2017**, *167* (6), 394−409.

(8) Cao, L.; Cui, X.; Hu, J.; Li, Z.; Choi, J. R.; Yang, Q.; Lin, M.; Hui, L. Y.; Xu, F. Advances in digital polymerase chain reaction (dPCR) and its emerging biomedical applications. *Biosens. Bioelectron.* **2017**, *90*, 459−474.

(9) Radmard, S.; Reid, S.; Ciryam, P.; Boubour, A.; Ho, N.; Zucker, J.; Sayre, D.; Greendyke, W. G.; Miko, B. A.; Pereira, M. R.; Whittier, S.; Green, D. A.; Thakur, K. T. Clinical utilization of the film Array meningitis/encephalitis (ME) multiplex polymerase chain reaction (PCR) assay. *Front. Neurol.* **2019**, *10*, No. 281.

(10) Wang, A. M.; Doyle, M. V.; Mark, D. F. Quantitation of mRNA by the polymerase chain reaction. *Proc. Natl. Acad. Sci. U.S.A.* **1989**, *86* (24), 9717−9721.
(11) Abudayyeh, O. O.; Gootenberg, J. S.; Konermann, S.; Joung, J.; Slaymaker, I. M.; Cox, D. B. T.; Shmakov, S.; Makarova, K. S.; Semenova, E.; Minakhin, L.; Severinov, K.; Regev, A.; Lander, E. S.; Koonin, E. V.; Zhang, F. C2c2 is a single-component programmable RNA-guided RNA-targeting CRISPR effector. *Science* **2016**, *353* (6299), No. aaf5573.
(12) Li, S. Y.; Cheng, Q. X.; Liu, J. K.; Nie, X. Q.; Zhao, G. P.; Wang, J. CRISPR-Cas12a has both cis- and trans-cleavage activities on single-stranded DNA. *Cell Res.* **2018**, *28* (4), 491−493.
(13) East-Seletsky, A.; O'Connell, M. R.; Knight, S. C.; Burstein, D.; Cate, J. H. D.; Tjian, R.; Doudna, J. A. Two distinct RNase activities of CRISPR-C2c2 enable guide-RNA processing and RNA detection. *Nature* **2016**, *538* (7624), 270−273.
(14) Teng, F.; Guo, L.; Cui, T.; Wang, X. G.; Xu, K.; Gao, Q.; Zhou, Q.; Li, W. CDetection: CRISPR-Cas12b-based DNA detection with sub-attomolar sensitivity and single-base specificity. *Genome Biol.* **2019**, *20* (1), No. 132.
(15) Chen, J. S.; Ma, E.; Harrington, L. B.; Da Costa, M.; Tian, X.; Palefsky, J. M.; Doudna, J. A. CRISPR-Cas12a target binding unleashes indiscriminate single-stranded DNase activity. *Science* **2018**, *360* (6387), 436−439.
(16) Gootenberg, J. S.; Abudayyeh, O. O.; Lee, J. W.; Essletzbichler, P.; Dy, A. J.; Joung, J.; Verdine, V.; Donghia, N.; Daringer, N. M.; Freije, C. A.; Myhrvold, C.; Bhattacharyya, R. P.; Livny, J.; Regev, A.; Koonin, E. V.; Hung, D. T.; Sabeti, P. C.; Collins, J. J.; Zhang, F. Nucleic acid detection with CRISPR-Cas13a/C2c2. *Science* **2017**, *356* (6336), 438−442.
(17) Zhou, H.; Bu, S.; Xu, Y.; Xue, L.; Li, Z.; Hao, Z.; Wan, J.; Tang, F. CRISPR/Cas13a combined with hybridization chain reaction for visual detection of influenza A (H1N1) virus. *Anal. Bioanal. Chem.* **2022**, *414* (29), 8437−8445.
(18) Peng, S.; Tan, Z.; Chen, S.; Lei, C.; Nie, Z. Integrating CRISPR-Cas12a with a DNA circuit as a generic sensing platform for amplified detection of microRNA. *Chem. Sci.* **2020**, *11* (28), 7362−7368.
(19) Wang, J.; Xia, Q.; Wu, J.; Lin, Y.; Ju, H. A sensitive electrochemical method for rapid detection of dengue virus by CRISPR/Cas13a-assisted catalytic hairpin assembly. *Anal. Chim. Acta* **2021**, *1187*, No. 339131.
(20) Zeng, R.; Xu, J.; Lu, L.; Lin, Q.; Huang, X.; Huang, L.; Li, M.; Tang, D. Photoelectrochemical bioanalysis of microRNA on yolk-in-shell Au@CdS based on the catalytic hairpin assembly-mediated CRISPR-Cas12a system. *Chem. Commun.* **2022**, *58* (54), 7562−7565.
(21) Gill, R.; Zayats, M.; Willner, I. Semiconductor quantum dots for bioanalysis. *Angew. Chem., Int. Ed.* **2008**, *47* (40), 7602−7625.
(22) Yang, Y. L.; Mao, G. B.; Ji, X. H.; He, Z. K. DNA-templated quantum dots and their applications in biosensors, bioimaging, and therapy. *J. Mater. Chem. B* **2020**, *8* (1), 9−17.
(23) Wang, G.; Li, Z.; Ma, N. Next-generation DNA-functionalized quantum dots as biological sensors. *ACS Chem. Biol.* **2018**, *13* (7), 1705−1713.
(24) Arvand, M.; Mirroshandel, A. A. Highly-sensitive aptasensor based on fluorescence resonance energy transfer between l-cysteine capped ZnS quantum dots and graphene oxide sheets for the determination of edifenphos fungicide. *Biosens. Bioelectron.* **2017**, *96*, 324−331.
(25) Wu, D.; Song, G.; Li, Z.; Zhang, T.; Wei, W.; Chen, M.; He, X.; Ma, N. A two-dimensional molecular beacon for mRNA-activated intelligent cancer theranostics. *Chem. Sci.* **2015**, *6* (7), 3839−3844.
(26) Tikhomirov, G.; Hoogland, S.; Lee, P. E.; Fischer, A.; Sargent, E. H.; Kelley, S. O. DNA-based programming of quantum dot valency, self-assembly and luminescence. *Nat. Nanotechnol.* **2011**, *6* (8), 485−490.
(27) Ma, Y. X.; Mao, G. B.; Huang, W. R.; Wu, G. Q.; Yin, W.; Ji, X. H.; Deng, Z. S.; Cai, Z. M.; Zhang, X. E.; He, Z. K.; Cui, Z. Q. Quantum dot nanobeacons for single RNA labeling and imaging. *J. Am. Chem. Soc.* **2019**, *141* (34), 13454−13458.
(28) Park, J. C.; Choi, S. Y.; Yang, M. Y.; Nan, L.; Na, H.; Lee, H. N.; Chung, H. J.; Hong, C. A.; Nam, Y. S. Subnanomolar FRET-based DNA assay using thermally stable phosphorothioated DNA-functionalized quantum dots. *ACS Appl. Mater. Interfaces* **2019**, *11* (37), 33525−33534.





https://doi.org/10.1021/acs.analchem.5c08146
*Anal. Chem.* XXXX, XXX, XXX−XXX